doi:10.1016/j.jmb.2006.05.042 J. Mol. Biol. (2006) 360, 907–920

JMB

Available online at www.sciencedirect.com

SCIENCE DIRECT®

ELSEVIER

Two-rung Model of a Left-handed β-Helix for Prions Explains Species Barrier and Strain Variation in Transmissible Spongiform Encephalopathies

J. P. M. Langedijk[1]*, G. Fuentes[2], R. Boshuizen[1] and A. M. J. J. Bonvin[2]

[1]*Pepscan Systems B.V. Lelystad, The Netherlands*

[2]*Department of NMR Spectroscopy, Bijvoet Center for Biomolecular Research Utrecht University Utrecht, The Netherlands*

**Corresponding author*

In this study, a new β-helical model is proposed that explains the species barrier and strain variation in transmissible spongiform encephalopathies. The left-handed β-helix serves as a structural model that can explain the seeded growth characteristics of β-sheet structure in PrP^{Sc} fibrils. Molecular dynamics simulations demonstrate that the left-handed β-helix is structurally more stable than the right-handed β-helix, with a higher β-sheet content during the simulation and a better distributed network of inter-strand backbone-backbone hydrogen bonds between parallel β-strands of different rungs. Multiple sequence alignments and homology modelling of prion sequences with different rungs of left-handed β-helices illustrate that the PrP region with the highest β-helical propensity (residues 105–143) can fold in just two rungs of a left-handed β-helix. Even if no other flanking sequence participates in the β-helix, the two rungs of a β-helix can give the growing fibril enough elevation to accommodate the rest of the PrP protein in a tight packing at the periphery of a trimeric β-helix. The folding of β-helices is driven by backbone–backbone hydrogen bonding and stacking of side-chains in adjacent rungs. The sequence and structure of the last rung at the fibril end with unprotected β-sheet edges selects the sequence of a complementary rung and dictates the folding of the new rung with optimal backbone hydrogen bonding and side-chain stacking. An important side-chain stack that facilitates the β-helical folding is between methionine residues 109 and 129, which explains their importance in the species barrier of prions. Because the PrP sequence is not evolutionarily optimised to fold in a β-helix, and because the β-helical fold shows very little sequence preference, alternative alignments are possible that result in a different rung able to select for an alternative complementary rung. A different top rung results in a new strain with different growth characteristics. Hence, in the present model, sequence variation and alternative alignments clarify the basis of the species barrier and strain specificity in PrP-based diseases.

Keywords: β-helix; prion; strain; CJD; BSE

Introduction

The mammalian prion protein (PrP) is associated with various forms of neurodegenerative disorders known as the transmissible spongiform encephalopathies (TSE)s, like sheep scrapie, bovine spongiform encephalopathy (BSE) and human Creutzfeld Jacob disease (CJD). Prions consist of misfolded prion protein (PrP^{Sc}) that can act as a template to catalyse a conformational conversion of the correctly folded native PrP protein (PrP^{C}). This leads to the template-driven replication of misfolded prions that grow into fibrils.[1] However, the infection-determining conformation

Abbreviations used: PrP, prion protein; huPrP, human PrP; PrP^{Sc}, misfolded prion protein; PrP^{C}, correctly folded native PrP protein; TSE, transmissible spongiform encephalopathy; BSE, bovine spongiform encephalopathy; CJD, human Creutzfeld Jacob disease; vCJD, human variant of CJD; MD, molecular dynamics.

E-mail address of the corresponding author: j.p.m.langedijk@pepscan.nl

still has to be elucidated. Knowledge of the PrP^{Sc} fibril structure is essential for the understanding of the mechanism of fibril formation. The available structural data on PrP are all based on the structure of the native monomeric or dimeric PrP^{c} that does not organize into fibrils.[2–5]

The C-terminal two-thirds of the PrP^{c} folds into a stable structure of three helices and two hydrogen-bonded β-strands. The N-terminal part is in random coil and does not seem to have a fixed structure, except for the octapeptide repeat region, which is partly solved.[6] Little is known about the structure of the misfolded prion protein. Because PrP^{Sc} is folded into insoluble fibrils, it will be very difficult to solve their structure by NMR or X-ray crystallography. Especially residues just N-terminal to the solved X-ray structure are thought to be involved in the fibril formation by participating in the transition to a PrP structure that contains more β-sheet than native PrP^{c}.[7–12] Beyond this, little is known about the structure of the PrP^{Sc} fibrils. X-ray diffraction studies of several kinds of amyloid fibrils have revealed a common cross-β structure, with β-strands running perpendicular to the fibre axis and hydrogen bonds in parallel, giving rise to the observed 4.75 Å reflection parallel with the fibre axis, which agrees with the topologically simplest class of β-sheet proteins: the parallel β-helix protein.[13] However, the type of β-structure in the fibril is still not known. Raman optical activity experiments and molecular dynamics (MD) studies suggested that the β-structures agree with a flat antiparallel β-sheet.[14,15] Using solid-state NMR and crystalline powder X-ray diffraction, many important features have been defined but a refined and objective general model for the amyloid fibril is not available.[16–19] Recent studies on the structure of fibrils from segments of HET-s and Sup35p prion proteins do suggest a common architecture for these amyloid fibrils.[20–23] The results of these studies suggest that a part of the prion protein folds into a parallel β-sheet. Small Sup35-based peptides fold into stable so-called dry steric zippers. Others have proposed that amyloid proteins and peptides, including PrP may fold into β-helices after conformational conversion of the native protein.[24–26] Several studies proposed that a part of PrP might fold as a right-handed or a left-handed β-helix.[27,28] Electron crystallography of 2D crystals of PrP 27–30 led to low-resolution projection maps of PrP^{Sc} that indicated that the prions may assemble into trimers of left-handed β-helices composed of four β-helical rungs per PrP^{sc} monomer.[28] Essentially, the left-handed β-helix agrees with the common architecture of a parallel β-sheet and can be considered as a triangular form of the dry steric zipper observed in Sup35p peptides. Moreover, the left-handed β-helix is in good agreement with the shape of the published 2D PrP^{sc} crystal projections maps obtained by negative stain electron microscopy.[28]

We have built models of both left-handed and right-handed β-helices and show, using MD simulations that the left-handed β-helix is favoured over the right-handed β-helix, as indicated by its structural stability and hydrogen bonding characteristics. On the basis of our models, we suggest how alternative alignments can explain several unsolved problems in the prion field, like species barrier and strain differences.

Results and Discussion

β-Helices

The left-handed β helix is formed by triangular progressive coils (rungs). Each rung is formed by three hexapeptide motifs, which results in an approximate 3-fold symmetry. Especially the fifth position of the hexapeptide (usually I, L, V) and, to a lesser extent, the third position are the only truly conserved residues: these point toward the inside of the β helix. Position 1, 2, 4 and 6 point outwards and are almost free to vary.[29] The hexapeptide motif is generally X-X- [STAVc] -X- [LIVf] - [GAED], where lower-case letters denote a lower incidence and X means any other residue. Proline residues are excluded at most positions except for the first one, where its occurrence is high.[28] Although aromatic side-chains like Phe are found at the first position, no aromatic stack is known in left-handed β-helices.

Because each rung is formed by three hexapeptides, this results in a rung of 18 residues. In some sequences, a residue is deleted at one or two of the turns, which can result in rungs of 17 or 16 residues, respectively. Moreover, the rungs can accommodate loops at the turns, which can increase the number of residues in the rung.

Right-handed β-helices are comprised of L-shaped rungs of 22–26 residues. The right-handed β -helix has more sequence restrictions, and algorithms have been developed to predict its fold.[30] Three large hydrophobic residues on the fifth position fill the centre of the helical core in the left-handed β helical rung, whereas all six side-chains point inward in the ring are large and hydrophobic (I, L, V, M, C, F, W, Y) in the right-handed β-helical rung. Because these residues come together and intercalate their side-chains, the sequence dependence is higher for the crowded, right-handed helical core compared with that of the core of the left-handed β-helix. In contrast to left-handed β-helices, right-handed β-helices can have internal aromatic stacks.

Several studies have suggested that peptides corresponding to the region between residues 89 and 143 of the prion protein, which are structurally unstable in the native protein,[31,32] can form β-rich fibrillar aggregates.[33–35] The smallest known prion peptide that forms β-rich fibrillar aggregates corresponds to residues 106–126 (including the AGAAA-AGA palindrome).[36–39]

The construction of a prion β-helix on the basis of homology modelling is not straightforward because the β-helical prion conformation is not a preferred fold for PrP but occurs only under particular

circumstances and preferably with the aid of a pre-existing "inoculate" prion β-helix that can act as a template. Moreover, the β-helical fold is relatively tolerant to variations of amino acids, and sequences that are not tolerated in the fold can spill out as loops at every turn. Therefore, many sequences can be threaded into a β-helical fold, which makes modelling of the correct structure a challenge. This tolerance of the β-helical fold for sequence variation may also allow for different valid alignments of a prion sequence.

Multiple sequence alignments were made of 16–26 amino acid stretches between PrP residues 89 and 143 with a collection of rungs from right-handed and left-handed β-helices. If residues flanking the 89–143 region do not contribute to the proposed β-helical region, a PrP^{Sc} monomer can contribute a maximum of three rungs to the fibril, according to the assumption of 16–26 residues per rung.

Right-handed β-helix

It was not possible to construct a satisfactory model with rungs of right-handed β-helices as templates. The Beta Wrap program could not predict a right-handed β-helix when the PrP sequence 89–146 or repetitions of this sequence were used as input.[30] On the basis of several optimal alignments that we made with sequences of Prp89-146 or 105–146 with right-handed β-helical structures, we have made two 3D models using the SWISS-MODEL protein modelling server. The first one was based on two rungs of 1BHE (residues 177–225, corresponding to rungs 4 and 5 of 1BHE). The second model was based on one rung of 1RMG (residues 177–198, rung 5 of 1RMG) and one rung of 1BHE (residues 204–225, rung 5 of 1BHE)[40] (see Supplementary Data Figure 1). Because it was not possible to satisfy some basic rules, e.g. hydrophobic residues and not Pro at positions 1, 3, 9, 11, 14 and 16,[41] the resulting rungs were unsatisfactory. Depending on the alignment that was used, the core of the helix was badly filled, or contained a charged residue, or a proline residue was at a disallowed position. In the case of model 1, a large loop had to be deleted between the two rungs. All solutions that were found with the loopsearch resulted in a β-helical rung with imperfect β-strand hydrogen bonding close to the anchor residues of the loop. The second model gave a good geometry of a right-handed β-helix and, therefore, this helix was used in the MD simulation.

Left-handed β-helix

For alignment of the human (h)PrP sequence with rungs of left-handed β-helices, the sequence of Prp 89-146 was divided into three stretches of 18 residues. The three hPrP sequence stretches were aligned with typical rungs of several left-handed β-helices. Residues hPrP105-124 aligned reasonably well with the left-handed β-helical rungs (Table 1). Especially the V122G123 motif is typical for left-handed β-helices. The third position of the hexapeptide motif that points inward into the helix were occupied by Ala and Thr, which have a high positional prevalence at this position. The Thr side-chain can hydrogen bond to the main chain carbonyl group at position 6. Occupation of the fifth position, which also points inward, was reasonable but not perfect. Two side-chains at position 5 were relatively small (Val and Ala), and therefore the left-handed β-helix core was not filled completely. However, the packing was much better compared with that of the right-handed β-helix rungs models. Alignments of hPrP 125-142 with the rungs were reasonable (Table 1). Only G127 was unfavourable at the third position of the hexapeptide motif but, due to the adjacent large side-chain of F141, the rung was filled adequately. It was not possible to make a satisfactory alignment of PrP 89-104 or PrP82-105 with the rungs that would match three X-X- [STAVc] - [LIVf] - [GAED] - X motifs. Therefore, just two β-helical rungs per monomeric unit may form the core of the PrP^{Sc} fibril. Fourier transform infrared spectroscopy indicated a higher content of β-sheet, which would suggest that more rungs per monomer will participate in the fibril.[28] However, in β-helices the amount of β-sheet measured by Fourier transform infrared spectroscopy is overestimated, due to the high content of hydrogen-bonded turns and loops.[42]

Apart from the architectural preference, another advantage of the left-handed β helix model is the possibility to shift one complete hexapeptide motif, resulting in an identical rung structure due to the triangular symmetry, as will be discussed later.

Table 1. Alignment of residues 105–143 of human PrP with several rungs of left-handed β-helices

rung1 THJ		–	P	**A**	A	**V**	G	D	D	**T**	F	I	G	M	Q	A	F	V	F					
rung2 THJ		–	K	**S**	K	**V**	G	N	N	**C**	V	L	E	P	R	S	A	A	I					
rung1 XAT		G	D	**T**	L	**I**	G	H	E	**V**	W	I	G	T	E	A	M	F	M					
rung2 XAT		P	G	**V**	R	**V**	G	H	G	**A**	I	I	G	S	R	A	L	V	T					
rung2 LXA		A	N	**A**	H	**I**	G	P	F	**C**	I	V	G	P	H	V	E	I	G					
rung3 LXA		E	G	**T**	V	**L**	K	S	H	**V**	V	V	N	G	H	T	K	I	G					
rung6 LXA		S	D	**N**	L	**L**	M	I	N	**A**	H	I	A	H	D	C	T	V	G					
rung7 LXA		N	R	**C**	I	**L**	A	N	N	**A**	T	L	A	G	H	V	S	V	D					
rung1 hm9		P	E	**V**	Q	**I**	E	A	N	**V**	I	L	K	G	Q	T	K	I	G					
rung2 hm9		A	E	**T**	V	**L**	T	N	G	**T**	Y	V	V	–	D	S	T	I	G					
rung3 hm9		A	G	**A**	V	**I**	T	N	N	**S**	M	I	E	E	S	S	V	A	D					
rung4 hm9		–	G	**V**	T	**V**	G	P	Y	**A**	H	I	R	P	N	S	S	L	G					
rung5 hm9		A	Q	**V**	H	**I**	G	N	F	**V**	E	V	K	G	S	S	I	G	E					
rung6 hm9		–	N	**T**	K	**A**	G	H	L	**T**	Y	I	G	–	N	C	E	V	G					
humanPrP	105	P	K	**T**	N	**M**	K	H	M	**A**	G	**A**	A	AaG	**A**	V	**V**	G	G	124				
	125	L	G	**G**	Y	**M**	L	G	S	**A**	M	**S**	R	P	I	**I**	H	**F**	G	S	143			

According to this alignment, $humanPrP_{105\text{-}124}$ forms the first rung and $humanPrP_{125\text{-}143}$ forms the second rung. Residues that are important for folding point toward the centre of the helix and are located at the third or fifth position of the hexapeptide motif (in bold). The methionine stack is underlined. Residue Ala118 in huPrP is indicated with a lower-case letter because it loops out at the turn.

Modelling

Several runs of model building were performed on the basis of two sequential rungs of different left-

handed β-helices using the SWISS-MODEL protein modelling server:[40,43] all returned with almost identical models. The final model of the two left-handed β-helical rungs for huPrP105-143 was based on homology modelling with rungs of 1LXA and 1HM9.[44,45] Four sequential hexapetides in rung 6 and part of rung 7 of 1LXA corresponding to residues 114–137 were used to build PrP105-130, and two sequential hexapeptides in rung 4 of 1HM9 corresponding to residues 328–339 were used to build PrP131-143 for an optimal orientation of hPrP Pro_{137} (Figure 1). Energy minimization was performed to optimise the geometries of the backbone and side-chains. Pro105 and Pro137 are at the only position of the hexapeptide motif (position 1) that is favourable for proline. The internal side-chain of Thr107 is able to hydrogen bond with the backbone. The internal side-chains of Val122 and Phe141 have a favourable internal side-chain stack observed in other left-handed β-helices.[46] A possible interaction can be found between Phe141 and Met129. An interesting feature of this β-helical model is the internal side-chain stack of Met109 and Met129 at the fifth position, which has been observed in several β-helices.[41,47,48] The stability of the Met-stack is believed to originate from the favourable interaction of sulphur atoms, which are highly polarizable and their electrophilic or nucleophilic nature depends on the environment. The sulphur stack may induce a dipole in the atom, which may explain the favourable stacking by dipole–dipole interactions. The critical role for the sulphur atoms in methionine is illustrated by the effect of the oxidation of methionine residues on fibril formation. Oxidation interferes with the formation of PrP fibrils, and this effect is more profound for hamster than for mouse Prp.[49]

In the folded PrP^c protein, the residues in haPrP involved in the important Met stack are either in the flexible region (Met109) or exposed in the extreme N-terminal part of the X-ray structure (Met129) and, therefore, both methionine residues are likely be affected by oxidation.

It is not known which methionine residues are actually oxidized. If all methionine residues are oxidized, this will greatly affect the formation of the hamster prion because, according to Table 2, haPrP has three internal methionine residues (Met109, Met129 and Met139, of which Met109 and Met129 form a methionine stack and are highly exposed in $haPrP^c$). Since, according to the β-helix model, there is no Met stack in the mouse fibril, the oxidation of methionine may have less effect on mouse PrP fibril formation.

Using the sequences of hamster, sheep and cow PrP, it is possible to build a β-helix model that is the same as the model based on the human amino acid sequence, but a different preferred alignment was chosen for the mouse PrP sequence (Table 2). Because mousePrP has Leu at position 109 (human PrP numbering) instead of Met, the rungs cannot form a favourable Met stack. Therefore, for the alignment of the mouse sequence, the first hexapeptide in the second rung was shifted one position, which resulted in the homologous internal stacking of Leu109 and Leu130. For this model, an extra residue was inserted into the loop between rungs 1 and 2, and a deletion was made at an allowed position (position 1) between G131 and S132 (huPrP numbering) in the first turn of the second rung (Table 2). Although this shift by one position results in less favourable backbone hydrogen bonding, the homologous Leu109, Leu130 stacking and the typical L130G131 motif are favourable (huPrP numbering).

Molecular dynamics simulations

In order to study the stability of the right-handed and left-handed β-helix models, 20 ns MD simulations were performed in explicit solvent (for details, see Materials and Methods). An analysis of atom positional root-mean-squared deviations (RMSD) from the starting models (see Supplementary Data Figure 2) indicates that the two systems have reached equilibrium after approximately 10 ns, although the right-handed β-helix system still shows an increase in the RMSD values. We therefore limit all subsequent analysis to the last 10 ns of the simulation and concentrate on the middle rungs only to avoid end effects. Average values for RMSDs from the starting models, secondary structure content and number of intramolecular hydrogen bonds are given in Table 3.

The RMSDs indicate clearly that the left-handed β-helix model is more stable, with the backbone of the middle rungs remaining within 0.20 nm from the starting conformation. The difference between right and left-handed β-helices is also very pronounced when only the β-sheets are considered (0.15(±0.03) nm for the left-handed model *versus* 0.30(±0.02) nm for the right-handed model). The increased stability of the left-handed β-helix compared to the right-handed model is further reflected in its increased secondary structure content (see Table 3). This increased stability, however, is not reflected in the non-bonded energies, which can be considered equal within fluctuations along the MD simulation (data not shown).

The evolution of the secondary structure content of the left-handed and the right-handed β-helix models is shown in Figure 2. The secondary structure elements were defined on the basis of the DSSP algorithm.[50] The secondary structure plot for the left-handed β-helix simulation (Figure 2(a)) shows that two of the three β-sheets of the left-handed β-helix are preserved. These include, in particular, the sheets in which the stacking methionine residues are located. The unstable β-sheet is composed of residues 113–116 and 132–135; and it did show the worst sequence alignment of the three, with 75% of the side-chains pointing inwards at positions 3 and 5 corresponding to small alanine residues. Interestingly, this observation is in line with solid-state NMR studies of a PrP peptide, which showed conformational variability at Gly114.[51] The conformations sampled in the MD simulation, which

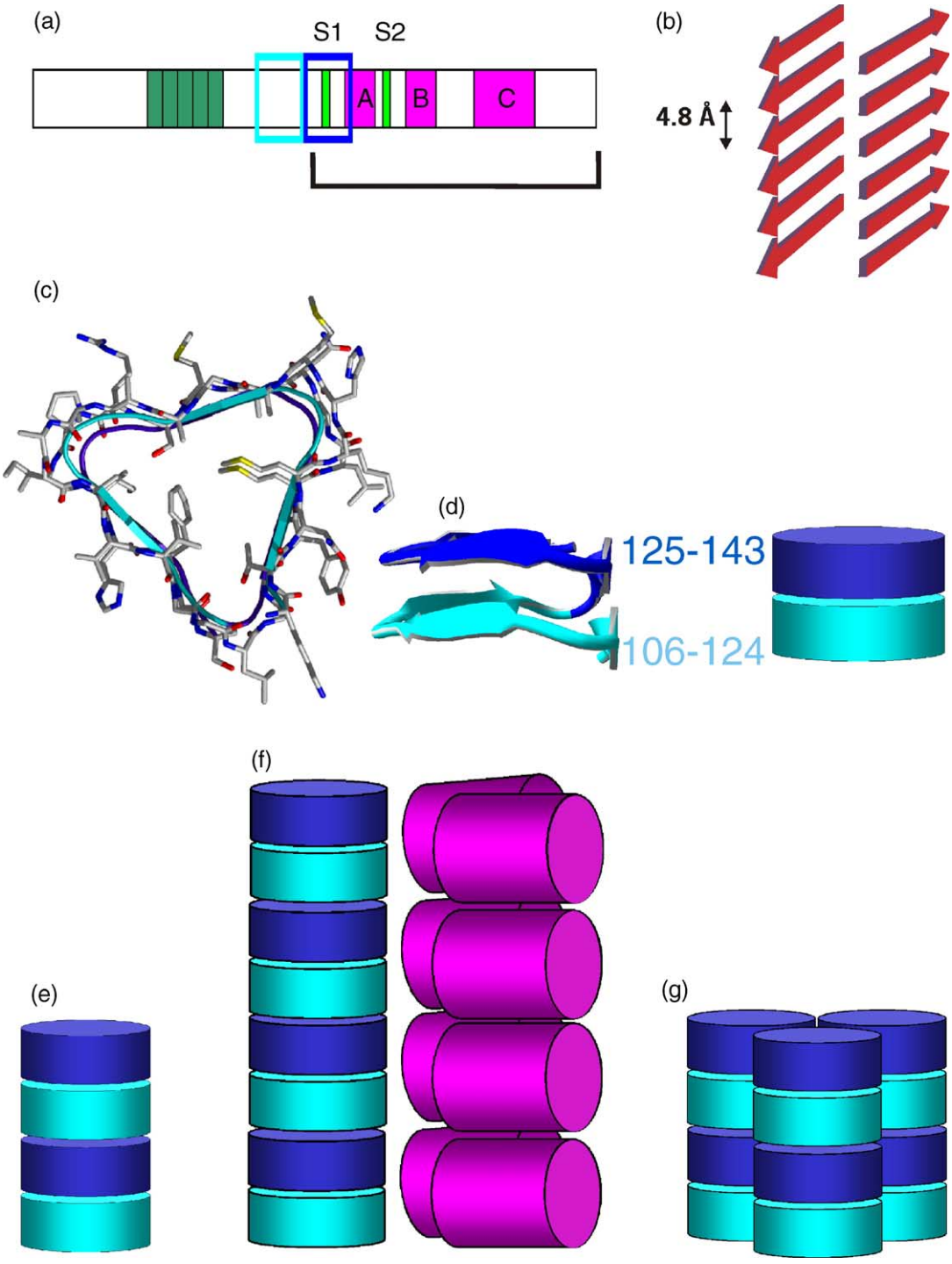

Figure 1. A representation of the PrP^C protein. (a) The part solved by X-ray crystallography and NMR is indicated by brackets, secondary structure elements are indicated: helices A, B and C in pink, β-strands S1 and S2 in light green, octarepeat regions in dark green. The region that refolds in two β-helical rungs is indicated with blue rectangles. (b) Representation of a dry steric zipper. (c) Top view of the 3D model of two left-handed β-helical rungs including side-chains. (d) The β-helical rung corresponding to $huPrP_{105\text{-}124}$ (cyan backbone) is stacked on top of the β-helical rung corresponding to $huPrP_{125\text{-}143}$ (dark blue backbone). Left: Side view of the 3D model without side-chains and (right) corresponding cartoon in which the rungs are represented as discs. (e) A stack of four rungs derived from two PrP monomers. (f) A stack of eight β-helical rungs and four pairs of C-terminal α-helices (residues 173–194 and 200–225) derived from four PrP monomers. (g) Trimer of stacked β-helical rungs.

contain two stable β-sheets, are reminiscent of the characteristic topology defined as a steric zipper (Figure 1(b)).

We also analysed the inter-strand hydrogen bonding: a hydrogen bond was considered to exist if the distance between the hydrogen atom and the

Table 2. Alignment of residues 105–143 of human, hamster, bovine and mouse PrP

HuPrP	rung 1	P K **T** N **M** K H M **A** G **A** A AaG **A** V **V** G
	rung 2	gL G **G** Y **M** L G S **A** M **S** R P I **I** H **F** G S
HamPrp	rung 1	P K **T** N **M** K H M **A** G **A** A AaG **A** V **V** G
	rung 2	gL G **G** Y **M** L G S **A** M **S** R P M **M** H **F** G N
BovPrP	rung 1	P K **T** N **M** K H V **A** G **A** A AaG **A** V **V** G
	rung 2	gL G **G** Y **M** L G S **A** M **S** R P L **I** H **F** G S
MoPrp	rung 1	P K **T** N **L** K H V **A** G **A** A AaG **A** V **V** G
	rung 2	glG G **Y** M **L** G - S **A** M **S** R P I **I** H **F** G N

Structurally important, inward pointing side-chains are printed in bold. The shifted hexapeptide in the mouse PrP alignment is underlined.

acceptor was less than 0.27 nm and the donor-hydrogen-acceptor angle was less than 60° (only hydrogen bonds with an occurrence above 25% are reported). In the case of the left-handed β helical rung, eight stable inter-strand backbone–backbone hydrogen bonds, parallel with the fibre axis, could be detected at different sides of the structure, while only one was observed in the right-handed model (Table 4). The larger number of hydrogen bonds and their increased stability (as monitored by their occurrence) in the left-handed model is consistent with a more defined structure fluctuating between a classical left-handed β-helix and a dry steric zipper. We have to note here, however, that our models correspond to only four rungs; longer constructs might well show much more increased stability and result in more dramatic differences between the right-handed and the left-handed models. Note that a second left-handed β-helix model was generated that was also subjected to MD simulation: it showed a stable structure similar to the first model (see Figure 3 and Tables 1 and 2 in the Supplementary Data). Another observation that favour the left-handed model is that, in the MD simulation of the right-handed model, arginine side-chains present in the centre of the rung are snorkelling to reach the solvent, thereby destabilizing the β-helix (data not shown); burial of a charge in the centre of our right-handed β-helix model is thus unfavourable.

Fibril architecture

A model of a fibril was built by stacking several of the left-handed two rungs models (Figure 1(d)). Because most left-handed β-helices are organized as trimers, and a trimeric assembly was observed in the 2D crystals,[28] the stacked PrP rungs were superimposed onto the trimer of 1LXA.[44] There are three different ways in which a triangular stack of rungs can be superimposed onto the β-helix in the trimer, but only two orientations position the positively charged residues at the periphery of the trimer. From these two possibilities, we chose the orientation that had a cluster of Met112 and Met134 pointed toward the centre of the trimer (Figure 3). The rationale for this choice was that the sulphur atoms and histidine111 could be involved in intermolecular contacts between neighbouring stacks in the trimer, or might be responsible for coordinating the uranyl atoms observed in the 2D crystals.[28] We refined the two possible trimer orientations using HADDOCK,[52] and characterized the interaction between the three β-helices: the trimer shown in Figure 3 is clearly the most favoured orientation with a higher buried surface area (1630^2 *versus* 984^2), a lower HADDOCK score (weighted sum of van der Waals, electrostatic and desolvation energies) (−59 *versus* −46) and the most favourable binding energy according to the DFIRE statistical potential (−20.6 kcal mol^{-1} *versus* −15.9 kcal mol^{-1}).[53] The proposed trimer model could be tested by mutating interface residues His111, Met112, Ser132, and Met134, and checking whether the ability to bind uranyl ions is affected.

To investigate whether a fibril with just two rungs per monomer could accommodate the remainder of PrP in the fibril, the C-terminal helices (residues 173–228) and the octarepeat region (residues 51–91) were placed at the edges of the β-helical trimer. To validate the possibility of the two-rung model, it is not necessary to postulate an accurate model for the orientation of the C-terminal α-helices B and C. Our objective is only to demonstrate that the helices, and the octarepeats, could somehow pack in such a way that they allow stacking of the next monomer in the growing fibril (Figure 1(f)). The elevation of two β-helical rungs (2×4.8=9.6) is comparable to the elevation of one α-helix (9.4) and to the approximate elevation established with four octarepeats (1.3×7.9=10.2). The fifth octarepeat (residues 84–91)

Table 3. Structural statistics from the MD simulations of the left- and right-handed β-helix models

A. Average backbone RMSD[a] with respect to the starting point

	Backbone	Heavy atoms	β-sheets	β-sheets (heavy atoms)
Left-handed β	0.20 (0.02)	0.30 (0.02)	0.15 (0.02)	0.20 (0.03)
Right-handed β	0.40 (0.05)	0.45 (0.04)	0.30 (0.02)	0.35 (0.03)

B. Secondary structure elements content[b] (%)

	Structure	β-sheet	Turn
Left-handed β	21 (4)	15 (5)	3 (1)
Right-handed β	10 (1)	9 (1)	7 (9)

C. Intramolecular hydrogen bonds

Left-handed β	16 (2)
Right-handed β	7 (2)

The analysis was performed on the middle two rungs. Averages over the 10–20 ns segment of the MD trajectories are reported together with standard deviations in parentheses.

[a] The backbone positional RMSD values were calculated with respect to the original models after superposition on the respective secondary structure element (β-sheet) backbone atoms of the middle rungs as defined by DSSP. (leftB: 128–129, 132–133, 141–142 in the first rung and 109–110, 115–116, 122–123 in the second one; right-: 128–130, 136–137 for the first rung and 106–108, 135–137 for the second rung).

[b] The secondary structure content was calculated using the DSSP algorithm on the two middle rungs.

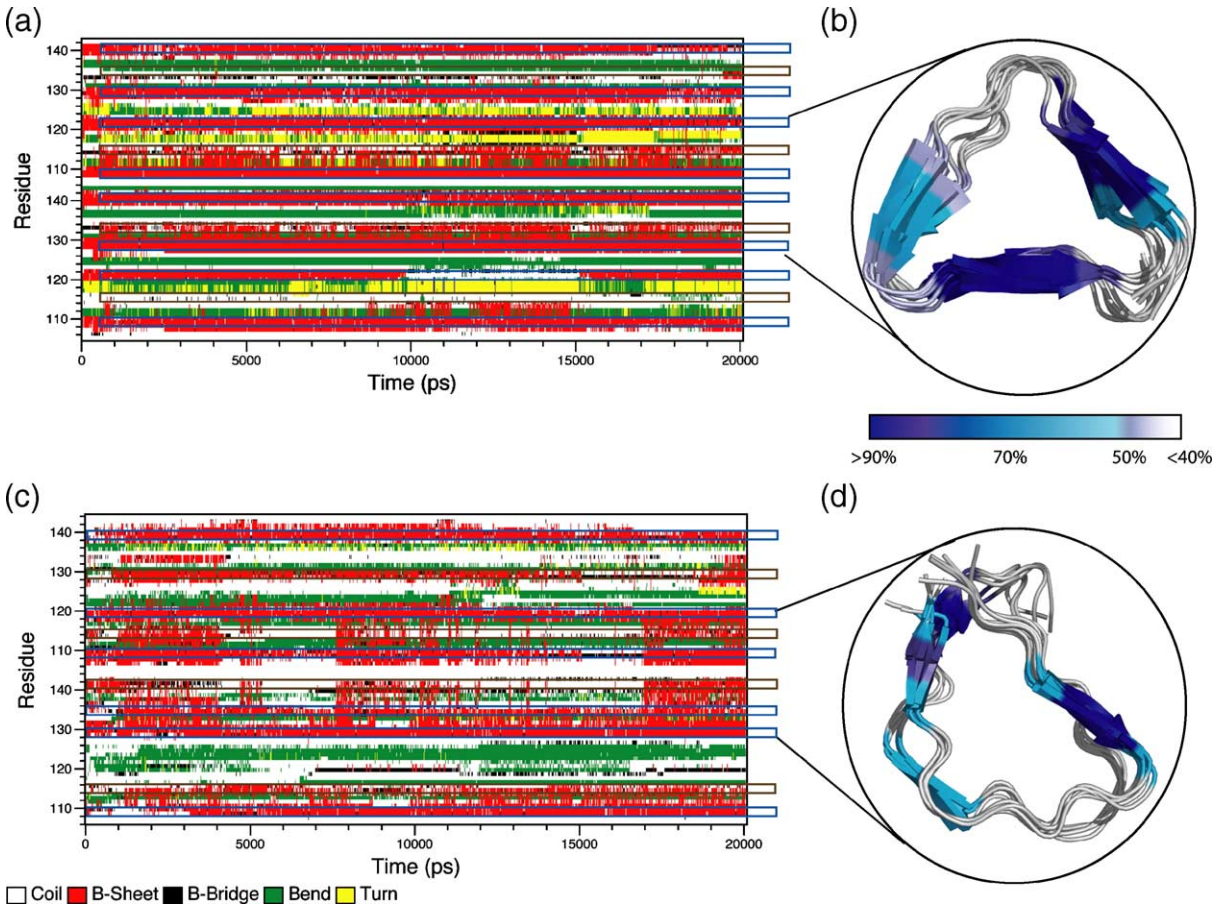

Figure 2. Plots of the secondary structure content as a function of the MD simulation time for (a) the left-handed and (c) the right-handed β-helix models. The most stable and well-conserved β-sheets are indicated by blue boxes and those with a lower populations are indicated by brown boxes. (b)–(d) Views of the corresponding two middle rungs (superposition of five snapshots taken from the last 1 ns of the simulations) are indicated on the right. The residues in the β-sheets are colour-coded according to the percentage of the simulation time they are found in the β-conformation.

could be part of the connection between octarepeats and the β-helix. These numbers indicate that our two-rung model could indeed accommodate the remainder of the PrP structure.

There are many possibilities to pack -helices (residues 173–228) in parallel or antiparallel fashion, which all have an elevation of just one α-helix per monomer. (Supplementary Data Figure 4) Especially, since the two-rung model does not have large loops at any triangular corner of the β-helical trimer, the α-helices can pack very close to the β-helix. Considering that helices are not rigid bodies but could somehow rearrange during the conformational conversion, even more packing alternatives are possible. An example of a fibril model of $PrP^{Sc}_{92\text{-}228}$ that allows just two rungs per monomer is shown in Figure 4. The elevation per monomer is limited, and the diameter of the fibril should match the measurements in the 2D crystals:[28] the diameter of our model fibril is approximately 70 , which is the same as the measured diameter of the polymer in the 2D crystal.

Compared to the model described by Govaerts *et al.*[28] which used four β-helical rungs per monomer, our two-rung fibril is much denser, with a tighter packing of helices and only half the elevation per monomer.

If only two rungs are involved, the model must be able to explain the electron density difference between the PrP27-30 oligomers and the "mini-prion" $PrP^{Sc}106$, with a deletion of the 141–176

Table 4. Interstrand backbone–backbone hydrogen bond statistics (10–20 ns)

Donor	Acceptor	Lifetime (%)
Left-handed β		
Leu125(A) N	Pro105(B) N	47
Leu130(A) N	Met109(B) O	42
Gly142(A) N	Gly126(A) O	25
Lys106(B) N	Gly126(A) O	89
His111(B) N	Leu130(A) O	52
Met112(B) N	Gly131(A) O	92
Gly124(B) N	Gly142(A) O	95
Leu125(B) N	Pro105(B) O	84
Right-handed		
Ser132(A) N	Ala113(B) N	50

The letters A and B stand for the first and second rungs used to build the models. Hydrogen bonds occurring between different sheets in the middle rungs, with a lifetime >25%.

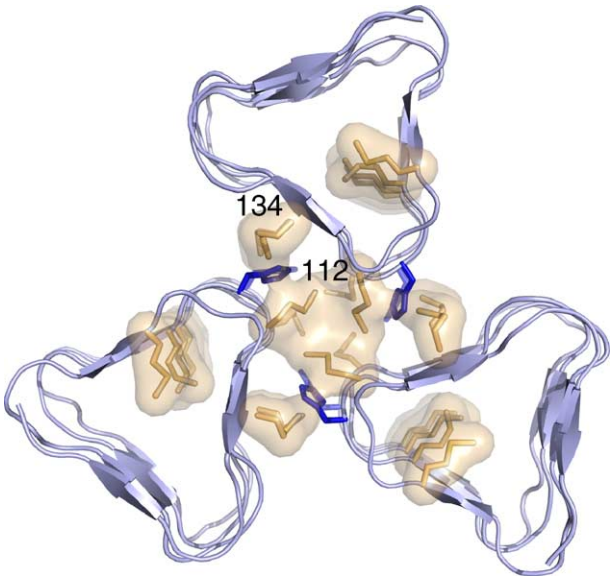

Figure 3. Trimer of β-helical rungs. Each PrP^{Sc} monomer contributes two β-helical rungs to the stack of four rungs. Internal side-chains of Met109, Met129 forming the Met-stack and external side-chains of Met112, Met134, and His111 forming the trimer interface are shown. All methionine residues are shown with transparent surfaces, His111 is shown in blue.

region.[28] According to the difference map, region 141–176 is located in a restricted area, which has the approximate dimensions of a β-helical rung. This suggests that the 141–173 region forms a β-helical rung. In Govaerts's model, deletion of these 36 residues (141–176) should delete a rung, as well as a very large loop, which must be just as big as the rung. However, such an extra deletion is not apparent from the difference map. Therefore, it is possible that residues 141–176 are not part of a rung but instead connect the β-helical rungs and the α-helices, and are thus spilled out between the β-helical rungs in the trimer (Figure 5). In Figure 6, the β-helical trimer is rotated 60° relative to the trimer centre of Govaerts's model. As a result, residues 141–176 are located in a loop and not in an additional β-helical rung (Figure 5(b)). A deletion of the 36 residue loop will result in a very short connection of several residues between the last rung of the β-helix and α-helix B, which will be shortened by five residues. This deletion can still result in an isomorphuous polymer for PrP27-30 and $PrP^{Sc}106$.[28] Therefore, the EM study, the better alignment of the two rungs compared with the four rungs, the methionine stack and the presence of His111 and Met112 in the trimer interface would favor the two-rung model over the four-rung model.

Further support for our fibril model comes from the fact that the residues in the β-helix and part of the connecting loop between the β-helix and α-helix B would be inaccessible for antibodies and proteolytic enzymes, while α-helices B and C and the carbohydrates would decorate the periphery of the trimeric β-helix and thus be able to bind antibodies. This would agree with the results of immunological studies.[7,54]

The two-rung model explains fibril stability and species barrier

The stacking of the side-chains of adjacent rungs in the interior of the parallel β-helix, which is important for its stability, may explain why individuals homozygous at codon 129 and especially homozygous for Met at position 129, have a higher susceptibility for prion infection. The Met109-Met129 stack is favourable because it can be continued endlessly in a growing two-rung fibril (Met109-Met129- Met109-Met129 etc.). This Met stack may explain the fact that most of the CJD and human variant CJD(vCJD) are homozygous for Met at codon 129. It may also explain the strong species barrier between e.g. human or hamster with Met at positions 109 and 129 and the mouse, which has Leu at position 109 and therefore cannot continue the Met-stack.[55] In contrast to mice, the related bank voles have a low species barrier,[56] which agrees with the occurrence of Met at position 109. As described above, an alternative alignment was favoured for the mouse PrP sequence, which was different from the PrP alignments of other species (Table 2). This alternative alignment explains that the over-expression of a mousePrP mutant with mutations to Met at positions 109 and 112 showed prolonged incubation times with several mouse strains: the mouse strains used for inoculation have an alternative alignment with a Leu109 - Leu 129-

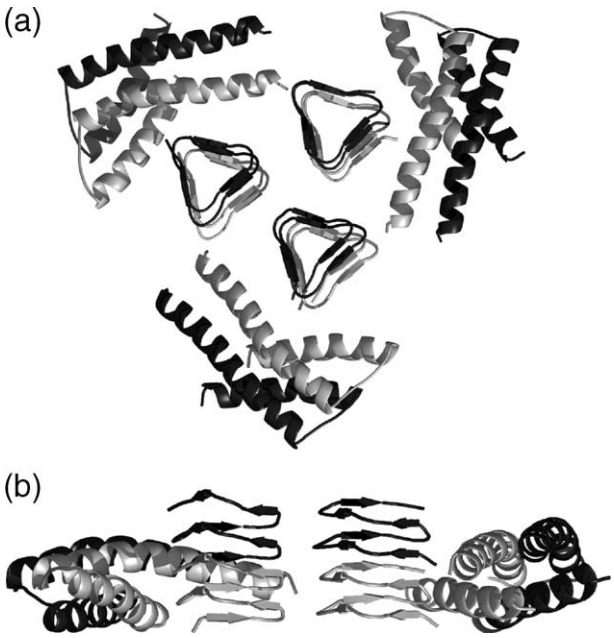

Figure 4. Top and side view of a slice of the huPrP27-30 ($huPrP_{92-228}$) fibril composed of two stacked $huPrP^{Sc}$ monomers organised as a trimer. The centre of the trimer is composed of the β-helical rungs in two shades. The C-terminal helices B and C are located at the periphery.

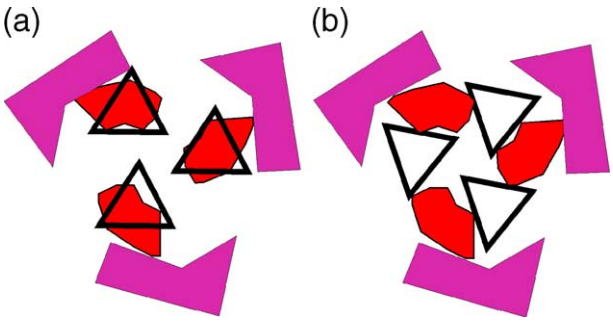

Figure 5. A representation of the difference map between complete PrP^{Sc} and a PrP^{Sc} without the 141–176 region according to Figure 3(b) of Govaerts *et al.*[28] in which the trimeric β-helices (triangles) can be mapped (a) on top of the 141–176 region (red) or (b) turned by 60° in order to position the β-helical rungs between the 141–176 regions. Pink rectangles illustrate the positions of helices B and C at the periphery.

stack, which is no longer compatible with the over-expressed mutant that contains Met109.[57]

This may explain why transgenic mice over-expressing human PrP with Val129 are not susceptible to vCJD: the fibril of the CJD-inoculate probably has a Met109-Met129-stack that cannot act as a good template for PrP with Val129 in the transgenic mice.[58] The importance of the Met-stack may explain why transgenic mice carrying the HuPrP allele encoding Val129 are not susceptible to CJD, and why chimeric transgenic mice carrying part of the HuPrP allele encoding Met129 are susceptible to CJD.[59] These explanations favour the prion-protein-only hypothesis and no longer require the support of an unknown factor X to explain this phenomenon.

In sheep prion, a susceptibility-linked polymorphism is located at position 133 (huPrP numbering). Sheep with Val133 are more susceptible to scrapie than sheep with Ala133.[60–62] In the alignment (e.g. see Tables 1 and 2), residue 133 is located at the third position of the hexapeptide motif, which is structurally important because the side-chain points in toward the helix. This third position shows the highest preference for Val in left-handed β-helices.[28,29] In the 3D model, the interior of the second rung will be better filled by a valine side-chain compared to a rung with alanine at position 133 (Figure 6). Therefore, the sheep PrP with Val133 probably has a higher tendency to form a β-helical fibril.

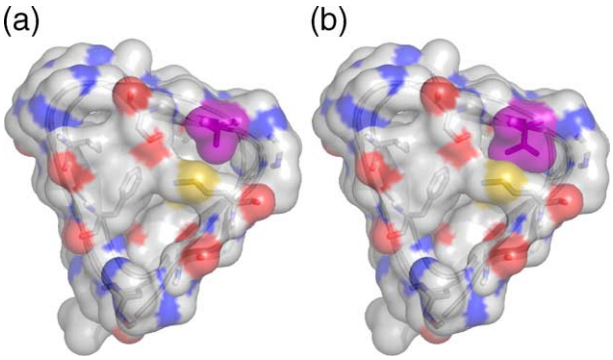

Figure 6. Top view of the 3D model of two left-handed β-helical rungs showing the internal side-chains. The β-helical rung corresponding to $huPrP_{125\text{-}143}$ is shown on top to illustrate the packing of (a) Ala133 compared to (b) Val133 in purple.

Alternative alignments and strain variation

Because the PrP protein has not evolved to fold as a β-helix, and because of the tolerance of the β-helical fold for sequence variation, there may be different possibilities to make a valid alignment of PrP with β-helical rungs. Just as the mutations in mouse PrP results in a different alignment, it is possible that even the same sequence can give rise to different alignments. Figure 7 shows three different presentations of human PrP rungs with an alternative alignment of the second rung, in which the first or second hexapeptide of the second rung is shifted. As a result, the structurally important inward-pointing side-chains are different; when the rung is at the end of the fibril, it will have a different capacity for acting as an alternative template. Although the architecture of the β-helical core is identical, this alternative template could have the most impact on the stability and growth characteristics of the fibril. In fact, a third

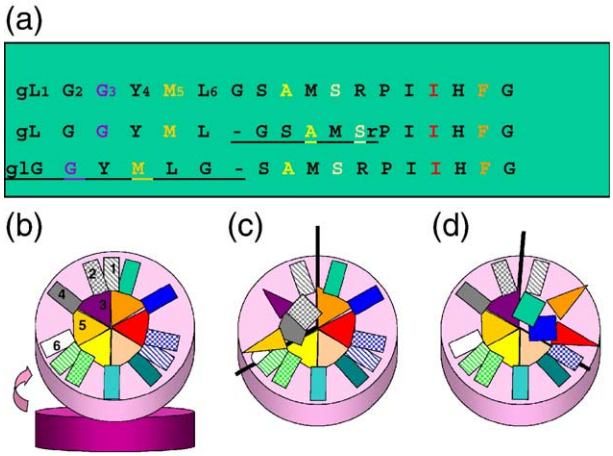

Figure 7. Examples of three different alignments of a β-helical rung of $PrP_{125\text{-}143}$ that all satisfy the sequence rules for a left-handed β-helical fold. (a) Residues that point inward the β-helical rung are coloured. (b) The cartoons display a perpendicular view of the top surface of a β-helical rung at the end of a growing fibril (in this case $PrP_{125\text{-}143}$). The first six residues of the rung are numbered in the alignment and in the cartoon. Twelve residues are pointing outward (rectangles) and six residues (triangles), coloured as in (a), are pointing inward. The cartoon shows that a shift of one residue of one hexapeptide in the alignment (underlined) has a large structural impact on one-third of the surface of the top ring (compare cartoons (b)–(d)). Although one of the alignments may be the preferred structure, other alignments are possible. The final choice for the alignment/structure of PrP will be dictated by the highest complementarity to the top ring of the incoming infecting strain.

of the surface of the β-helical rung is changed completely (Figure 7(b)). Therefore, without codon polymorphism or differences in glycosylation, it is still possible to generate different prion strains with the same PrP sequence. Apart from the effect on the stacking of the rungs at the end of the growing fibril, some side-chains that switch from internal to external positions in the alternative alignment will result in different surface properties of the side of the β-helical trimer; this, in turn, might affect the packing of the remainder of the PrP polypeptide. In addition, the protein chain N-terminal to Pro105 will be in a different environment. This may have an effect on the proteolytic cleavage site of PrP^{Sc}, which is different for different strains.[63] Apart from the top rung template, strain variation may be explained by the number of rungs per PrP^{Sc} monomer, PrP regions outside the β-helical rungs, or the multimeric organisation (dimeric or trimeric) of the β-helices as suggested by Govaerts *et al.*[28]

As was suggested for mousePrP, mutations can have impact on the alignment (Table 2). An interesting case is the Pro102 to Leu102 mutation, which leads to spontaneous fibril formation in humans with Gerstmann-Straussler-Scheinker (GSS) disease. This mutation allows an extra hexapeptide in the β-helical fold. The mutation can result in an alternative alignment shifted by one hexapeptide with an additional favourable stack of Leu102 and Val122, and better backbone–backbone hydrogen bonding (Figure 8(a)). The chance of alternative folds is increased with the addition of an extra favourable hexapeptide motif: the alignment can incorporate seven hexapeptide regions (including both the 98–104 and the 137–143 hexapeptides) and a hexapeptide shift can lead to a repetition of seven different rungs (Figure 8(b)). This model does not have the continuous Met stack anymore but has two different interrupted internal Met-stacks. (In the case of the hamster sequence, there will even be a third interrupted external Met stack). This alignment has very favourable side-chains at the fifth position (L, V, F, A, M, M, M). However, it is not likely that a stable trimer of β-helices will form if all seven hexapeptides are used continuously as shown in the alignment of Figure 8(b). In the case of six hexapeptides in the two-rung model, the protein chain enters the β-helical triangle at the same corner as it leaves the triangle (Figure 8(c), top). In contrast, when seven hexapeptides are used, the entrance and exit of the protein chain are at different corners; an exit at the centre corner will not allow trimerization (Figure 8(c), bottom). In order to retain a trimer of β-helices, the alternative alignment involving seven hexapeptides may be possible, but a hexapeptide motif in the alignment has to be skipped intermittently to allow exit of the protein chain at the periphery of the β-helical trimer at one of the alternative triangular corners. This may actually block the formation of a mature fibril or result in an unstable fibril prone to branching and breaking, which will result in the expansion of the number of templates that can act as new nuclei leading to disease progression. Prion fibrils of PrP(P102L) are indeed more sensitive to protease digestion.[64]

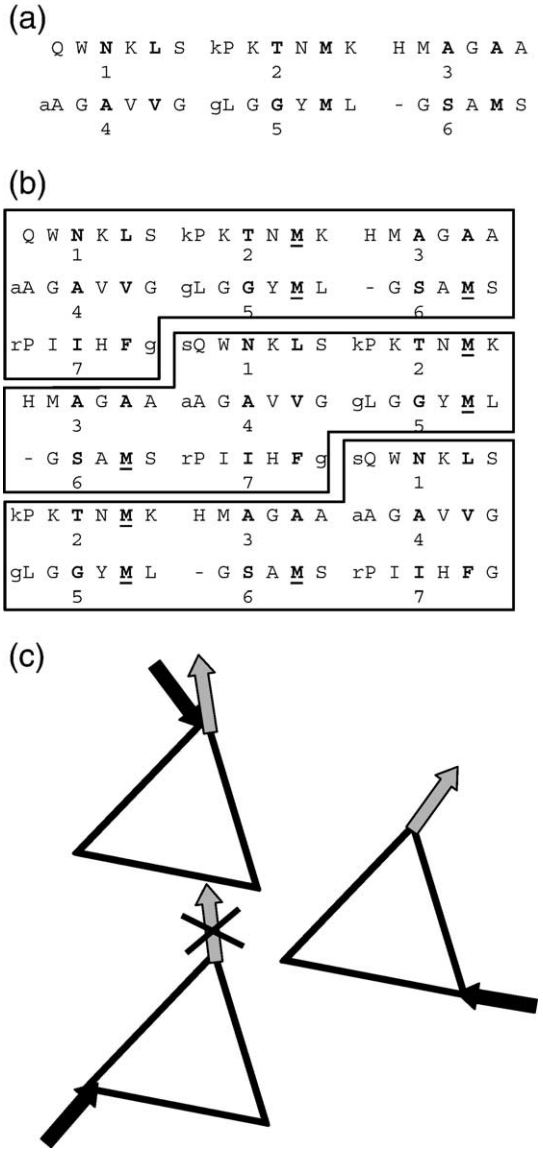

Figure 8. Alternative alignment of huPrP98-136. As a consequence of the mutation of Pro102 to Leu102 in GSS patients, the 98–103 hexapeptide motif satisfies the sequence rules for a left-handed β-helix. As a consequence, the alignment is shifted by one hexapeptide motif relative to the alignment in Figure 1. Alignment is possible with (a) addition of the N-terminal hexapeptide motif and deletion of the C-terminal hexapeptide motif, or (b) the addition of an N-terminal hexapeptide motif resulting in a repetition of seven hexapeptides. The methionine stack is underlined, the hexapeptides are numbered and each set of seven hexapeptide motifs is boxed. Arrows in (c) indicate the incoming and outgoing protein chain in the β-helical triangles of the trimer. The alternatives are the result of inclusion of an extra hexapeptide motif in the rung. The example at the bottom does not allow trimerization.

In mice, the Pro101 to Leu101 mutation is not enough to produce a spontaneous prion disease,[65] but the mutation does influence the incubation time

in these so-called 101LL mice for different TSEs that may be explained by the alignment of the rung templates. Inoculation of GSS in 101LL mice resulted in a shorter incubation time than in wild-type (wt) mice, which is explained by the higher degree of compatibility with the 101LL sequence, compared with the wt sequence (Figure 9(a) compared to (b)). With the 101LL sequence, it is possible to generate a rung with perfect backbone–backbone hydrogen bonding and a stack with Met129 (Figure 9(a)). With the wt sequence, however, the degree of compatibility is less and two positive charges of wt mPrP Arg135 and Lys109 of the inoculate are in close proximity, which is unfavourable (Figure 9(b)).

The β-helical model will be helpful for future research. It can be validated by testing the fibrillization of cyclic peptides compared to linear peptides corresponding to the postulated helical rungs. Assays using a mixture of rungs may demonstrate cooperativity in fibrillization. Mutations can be introduced into PrP that may affect staining for electron microscopy, species barrier or strain variation according to the β-helical two-rung model.

As proposed by Chien *et al*.[66] strain variation and species barrier are both manifestations of the same phenomenon: the ability of PrP to misfold into multiple self-propagating conformations. In this model, the templates that are formed by the terminal rungs dictate the folding of the next rung. The unprotected β-edges will be a strong driving force and sustain the propagation of the fibril. The unprotected β-edges allow the incorporation of a new rung by making hydrogen bridges with the next rung if the complementary side-chains allow this. Some side-chain stackings will be more favourable then others. The sulphur stack in Met109 and Met129 may be particularly favourable. Although the MD simulations have demonstrated that the β-structure is relatively stable, one of the three sheets of the left-handed β-helix shows a lower β-structure population, resembling more the so-called dry β-zipper.[23] However, our theory for the explanation of the species barrier and strain variation applies also for other parallel β-structures that include a methionine stack.

(a)

```
101LLmouse   Q W N K L SkP K T N L K H V A G A A
             aA G A V V GgL G G Y M L G S A M S R
Inoc.        Q W N K L SkP K T N M K H M A G A A
P102L GSS    aA G A V V GgL G G Y M L G S A M S R
```

(b)

```
Wtmouse      P K T N L K H V A G A A AaG A V V G G
           L G G Y M L G - S A M S R P M I H F G N
Inoc.        Q W N K L SkP K T N M K H M A G A A
P102L GSS    AaG A V V GgL G G Y M L G S A M S R
```

Figure 9. Alignments of the PrP sequence of inoculated mouse (101LL mouse or wt mouse) above and the sequence of the inoculum (P102L GSS) below. Basic residues with repulsive charges are boxed.

The preorganized β-helical templates at the end of the fibril dictate whether the next recruited rung will fold onto the template, and different templates can select for multiple infectious conformations. Therefore, it is the template that determines the strain. This study illustrates that, even with the same amino acid sequence, it is possible to generate multiple templates and changes in protein sequence can modulate the spectrum of favoured fibril conformations.

Material and Methods

Sequence analysis

Multiple sequence alignments were edited using MegAlign (DNASTAR Inc.). Secondary structure predictions were performed using the neural network-based program PHD and the threading program TOPITS.[67,68] Multiple sequence alignments were performed using several representative sequences of right-handed β-helical family members of known structure (PDB ID codes **1RMG**, **1DAB**, **1AIR**, and **1BHE**, and proposed rungs of SLpB)[41] and left-handed β-helical family members of known structure (PDB ID codes **1THJ**, **1XAT**, **1LXA**, 1HM9). Model building and visualisation was done with DeepView (SwissPDBViewer) 3.7 and SwissModel. [43,69] For one loop that could not be created automatically, the program LOOP SEARCH in the SYBYL package was used (Tripos Associates, St. Louis, MO). Model verification was carried out using WhatCheck.[70]

Amino acid numbering of all PrP species is based on the human PrP sequence.

MD simulations

All simulations were performed with the GROMACS 3.1.3 molecular dynamics package,[71] using the GROMOS 43a3 force field.[72] Starting structures of the left-handed and right-handed β-helices were solvated individually in truncated octahedron boxes, filled with 24312 and 24924 SPC water molecules,[73] and six and four additional chlorine ions to electro-neutralize the system, respectively.

Solute, solvent and counterions were weakly coupled independently to reference temperature baths at 300 K ($\tau = 0.1$ ps).[74] The pressure was maintained by coupling the system weakly to an external pressure bath at one atmosphere (one atmosphere = 101,325 Pa). The LINCS algorithm was used to constrain bond lengths, allowing an integration time step of 2 fs to be used.[75] The non-bonded interactions were calculated with a twin-range cut-off of 0.8 and 1.4 nm.[76] The long-range electrostatic interactions beyond the 1.4 nm cut-off were treated with the generalized reaction field model, using a dielectric constant of 54.[77] The non-bonded interaction pair list was updated every five steps. (For further details, see Hsu and Bonvin).[78]

Trajectory coordinates and energies were stored at 0.5 ps intervals. The analysis was performed using the set of programs within GROMACS.

Refinement of the trimer model with HADDOCK

The two trimer models were refined with HADDOCK.[52] Non-bonded interactions were calculated with a 8.5 Å cut-off using the OPLS non-bonded parameters.[79] The

refinement consisted of two short simulated annealing stages in torsion angle space, at first allowing flexibility only in the side-chains (500 integration steps from 500 K to 50 K) and then in the entire structure (500 integration steps from 300 K to 50 K). This was followed by refinement in an explicit water shell (3×100 MD steps at 100 K, 200 K and 300 K, followed by 1250 MD steps at 300 K, and a final cooling stage of 500 MD steps at 300 K, 200 K and 100 K). The resulting structures were subjected to a final steepest descent energy minimization.

Acknowledgements

This work was supported by a grant from the European Commission (QLK3-CT-2001-00283). We thank Puck Knipscheer for graphic assistance, Rob Meloen and Jan Langeveld for critically reading the manuscript. Dr Fuentes acknowledges the European Community (6th Framework Marie Curie grant Meif-ct-2003-501495) for financial support.

Supplementary Data

Supplementary data associated with this article can be found, in the online version, at doi:10.1016/j.jmb.2006.05.042

References

1. Collinge, J. (2001). Prion diseases of humans and animals: their causes and molecular basis. *Annu. Rev. Neurosci.* **24**, 519–550.
2. Riek, R., Hornemann, S., Wider, G., Billeter, M., Glockshuber, R. & Wuthrich, K. (1996). NMR structure of the mouse prion protein domain PrP(121-321). *Nature*, **382**, 180–182.
3. Donne, D. G., Viles, J. H., Groth, D., Mehlhorn, I., James, T. L., Cohen, F. E., Prusiner, S. B., Wright, P. E. & Dyson, H. J. (1997). Structure of the recombinant full-length hamster prion protein PrP(29-231): the N terminus is highly flexible. *Proc. Natl Acad. Sci. USA*, **94**, 13452–13457.
4. Knaus, K. J., Morillas, M., Swietnicki, W., Malone, M., Surewicz, W. K. & Yee, V. C. (2001). Crystal structure of the human prion protein reveals a mechanism for oligomerization. *Nature Struct. Biol.* **8**, 770–774.
5. Zahn, R., Liu, A., Luhrs, T., Riek, R., von Schroetter, C., Lopez, F. *et al.* (2000). NMR solution structure of the human prion protein. *Proc. Natl Acad. Sci. USA*, **97**, 145–150.
6. Zahn, R. (2003). The octapeptide repeats in mammalian prion protein constitute a pH-dependent folding and aggregation site. *J. Mol. Biol.* **334**, 477–488.
7. Peretz, D., Williamson, R. A., Matsunaga, Y., Serban, H., Pinilla, C., Bastidas, R. B. *et al.* (1997). A conformational transition at the N terminus of the prion protein features in formation of the scrapie isoform. *J. Mol. Biol.* **273**, 614–622.
8. Speare, J. O., Rush, T. S., III, Bloom, M. E. & Caughey, B. (2003). The role of helix 1 aspartates and salt bridges in the stability and conversion of prion protein. *J. Biol. Chem.* **278**, 12522–12529.
9. Torrent, J., Alvarez-Martinez, M. T., Liautard, J. P., Balny, C. & Lange, R. (2005). The role of the 132-160 region in prion protein conformational transitions. *Protein Sci.* **14**, 956–967.
10. Viles, J. H., Donne, D., Kroon, G., Prusiner, S. B., Cohen, F. E., Dyson, H. J. & Wright, P. E. (2001). Local structural plasticity of the prion protein. Analysis of NMR relaxation dynamics. *Biochemistry*, **40**, 2743–2753.
11. Caughey, B. W., Dong, A., Bhat, K. S., Ernst, D., Hayes, S. F. & Caughey, W. S. (1991). Secondary structure analysis of the scrapie-associated protein PrP 27-30 in water by infrared spectroscopy. *Biochemistry*, **30**, 7672–7680.
12. Pan, K. M., Baldwin, M., Nguyen, J., Gasset, M., Serban, A., Groth, D. *et al.* (1993). Conversion of alpha-helices into beta-sheets features in the formation of the scrapie prion proteins. *Proc. Natl Acad. Sci. USA*, **90**, 10962–10966.
13. Jenkins, J. & Pickersgill, R. (2001). The architecture of parallel beta-helices and related folds. *Prog. Biophys. Mol. Biol.* **77**, 111–175.
14. McColl, I. H., Blanch, E. W., Gill, A. C., Rhie, A. G., Ritchie, M. A., Hecht, L. *et al.* (2003). A new perspective on beta-sheet structures using vibrational Raman optical activity: from poly(L-lysine) to the prion protein. *J. Am. Chem. Soc.* **125**, 10019–10026.
15. DeMarco, M. L. & Daggett, V. (2004). From conversion to aggregation: protofibril formation of the prion protein. *Proc. Natl Acad. Sci. USA*, **101**, 2293–2298.
16. Diaz-Avalos, R., Long, C., Fontano, E., Balbirnie, M., Grothe, R., Eisenberg, D. & Caspar, D. L. (2003). Cross-beta order and diversity in nanocrystals of an amyloid-forming peptide. *J. Mol. Biol.* **330**, 1165–1175.
17. Balbirnie, M., Grothe, R. & Eisenberg, D. S. (2001). An amyloid-forming peptide from the yeast prion Sup35 reveals a dehydrated beta-sheet structure for amyloid. *Proc. Natl Acad. Sci. USA*, **98**, 2375–2380.
18. Benzinger, T. L., Gregory, D. M., Burkoth, T. S., Miller-Auer, H., Lynn, D. G., Botto, R. E. & Meredith, S. C. (1998). Propagating structure of Alzheimer's beta-amyloid(10-35) is parallel beta-sheet with residues in exact register. *Proc. Natl Acad. Sci. USA*, **95**, 13407–13412.
19. Jaroniec, C. P., MacPhee, C. E., Astrof, N. S., Dobson, C. M. & Griffin, R. G. (2002). Molecular conformation of a peptide fragment of transthyretin in an amyloid fibril. *Proc. Natl Acad. Sci. USA*, **99**, 16748–51673.
20. Tanaka, M., Chien, P., Yonekura, K. & Weissman, J. S. (2005). Mechanism of cross-species prion transmission: an infectious conformation compatible with two highly divergent yeast prion proteins. *Cell*, **121**, 49–62.
21. Krishnan, R. & Lindquist, S. L. (2005). Structural insights into a yeast prion illuminate nucleation and strain diversity. *Nature*, **435**, 765–772.
22. Ritter, C., Maddelein, M. L., Siemer, A. B., Luhrs, T., Ernst, M., Meier, B. H., Saupe, S. J. & Riek, R. (2005). Correlation of structural elements and infectivity of the HET-s prion. *Nature*, **435**, 844–848.
23. Nelson, R., Sawaya, M. R., Balbirnie, M., Madsen, A. O., Riekel, C., Grothe, R. & Eisenberg, D. (2005). Structure of the cross-beta spine of amyloid-like fibrils. *Nature*, **435**, 773–778.
24. Perutz, M. F., Finch, J. T., Berriman, J. & Lesk, A. (2002). Amyloid fibers are water-filled nanotubes. *Proc. Natl Acad. Sci. USA*, **99**, 5591–5595.
25. Lazo, N. D. & Downing, D. T. (1998). Amyloid fibrils may be assembled from beta-helical protofibrils. *Biochemistry*, **37**, 1731–1735.

26. Wetzel, R. (2002). Ideas of order for amyloid fibril structure. *Structure (Camb)*, **10**, 1031–1036.
27. Wille, H., Michelitsch, M. D., Guenebaut, V., Supattapone, S., Serban, A., Cohen, F. E. *et al.* (2002). Structural studies of the scrapie prion protein by electron crystallography. *Proc. Natl Acad. Sci. USA*, **99**, 3563–3568.
28. Govaerts, C., Wille, H., Prusiner, S. B. & Cohen, F. E. (2004). Evidence for assembly of prions with left-handed beta-helices into trimers. *Proc. Natl Acad. Sci. USA*, **101**, 8342–8347.
29. Parisi, G., Fornasari, M. S. & Echave, J. (2004). Dynactins p25 and p27 are predicted to adopt the LbetaH fold. *FEBS Letters*, **562**, 1–4.
30. Bradley, P., Cowen, L., Menke, M., King, J. & Berger, B. (2001). BETAWRAP: successful prediction of parallel beta -helices from primary sequence reveals an association with many microbial pathogens. *Proc. Natl Acad. Sci. USA*, **98**, 14819–14824.
31. Barducci, A., Chelli, R., Procacci, P. & Schettino, V. (2005). Misfolding pathways of the prion protein probed by molecular dynamics simulations. *Biophys. J.* **88**, 1334–1343.
32. Ziegler, J., Sticht, H., Marx, U. C., Muller, W., Rosch, P. & Schwarzinger, S. (2003). CD and NMR studies of prion protein (PrP) helix 1. Novel implications for its role in the PrPC–>PrPSc conversion process. *J. Biol. Chem.* **278**, 50175–50181.
33. Laws, D. D., Bitter, H. M., Liu, K., Ball, H. L., Kaneko, K., Wille, H. *et al.* (2001). Solid-state NMR studies of the secondary structure of a mutant prion protein fragment of 55 residues that induces neurodegeneration. *Proc. Natl Acad. Sci. USA*, **98**, 11686–11690.
34. Salmona, M., Morbin, M., Massignan, T., Colombo, L., Mazzoleni, G., Capobianco, R. *et al.* (2003). Structural properties of Gerstmann-Straussler-Scheinker disease amyloid protein. *J. Biol. Chem.* **278**, 48146–48153.
35. Tagliavini, F., Prelli, F., Porro, M., Rossi, G., Giaccone, G., Farlow, M. R. *et al.* (1994). Amyloid fibrils in Gerstmann-Straussler-Scheinker disease (Indiana and Swedish kindreds) express only PrP peptides encoded by the mutant allele. *Cell*, **79**, 695–703.
36. Boshuizen, R. S., Langeveld, J. P., Salmona, M., Williams, A., Meloen, R. H. & Langedijk, J. P. (2004). An in vitro screening assay based on synthetic prion protein peptides for identification of fibril-interfering compounds. *Anal. Biochem.* **333**, 372–380.
37. De Gioia, L., Selvaggini, C., Ghibaudi, E., Diomede, L., Bugiani, O., Forloni, G. *et al.* (1994). Conformational polymorphism of the amyloidogenic and neurotoxic peptide homologous to residues 106-126 of the prion protein. *J. Biol. Chem.* **269**, 7859–7862.
38. Forloni, G., Angeretti, N., Chiesa, R., Monzani, E., Salmona, M., Bugiani, O. & Tagliavini, F. (1993). Neurotoxicity of a prion protein fragment. *Nature*, **362**, 543–546.
39. Gasset, M., Baldwin, M. A., Lloyd, D. H., Gabriel, J. M., Holtzman, D. M., Cohen, F. *et al.* (1992). Predicted alpha-helical regions of the prion protein when synthesized as peptides form amyloid. *Proc. Natl Acad. Sci. USA*, **89**, 10940–10944.
40. Schwede, T., Kopp, J., Guex, N. & Peitsch, M. C. (2003). SWISS-MODEL: An automated protein homology-modeling server. *Nucl. Acids Res.* **31**, 3381–3385.
41. Jing, H., Takagi, J., Liu, J. H., Lindgren, S., Zhang, R. G., Joachimiak, A. *et al.* (2002). Archaeal surface layer proteins contain beta propeller, PKD, and beta helix domains and are related to metazoan cell surface proteins. *Structure (Camb)*, **10**, 1453–1464.
42. Freiberg, A., Morona, R., Van den Bosch, L., Jung, C., Behlke, J., Carlin, N. *et al.* (2003). The tailspike protein of Shigella phage Sf6. A structural homolog of Salmonella phage P22 tailspike protein without sequence similarity in the beta-helix domain. *J. Biol. Chem.* **278**, 1542–1548.
43. Guex, N. & Peitsch, M. C. (1997). SWISS-MODEL and the Swiss-PdbViewer: an environment for comparative protein modeling. *Electrophoresis*, **18**, 2714–2723.
44. Raetz, C. R. & Roderick, S. L. (1995). A left-handed parallel beta helix in the structure of UDP-*N*-acetylglucosamine acyltransferase. *Science*, **270**, 997–1000.
45. Sulzenbacher, G., Gal, L., Peneff, C., Fassy, F. & Bourne, Y. (2001). Crystal structure of Streptococcus pneumoniae *N*-acetylglucosamine-1-phosphate uridyltransferase bound to acetyl-coenzyme A reveals a novel active site architecture. *J. Biol. Chem.* **276**, 11844–11851.
46. Beaman, T. W., Sugantino, M. & Roderick, S. L. (1998). Structure of the hexapeptide xenobiotic acetyltransferase from *Pseudomonas aeruginosa*. *Biochemistry*, **37**, 6689–6696.
47. Pickersgill, R., Smith, D., Worboys, K. & Jenkins, J. (1998). Crystal structure of polygalacturonase from *Erwinia carotovora* ssp. *carotovora*. *J. Biol. Chem.* **273**, 24660–24664.
48. Huang, W., Matte, A., Li, Y., Kim, Y. S., Linhardt, R. J., Su, H. & Cygler, M. (1999). Crystal structure of chondroitinase B from Flavobacterium heparinum and its complex with a disaccharide product at 1.7 Å resolution. *J. Mol. Biol.* **294**, 1257–1269.
49. Breydo, L., Bocharova, O. V., Makarava, N., Salnikov, V. V., Anderson, M. & Baskakov, I. V. (2005). Methionine oxidation interferes with conversion of the prion protein into the fibrillar proteinase K-resistant conformation. *Biochemistry*, **44**, 15534–15543.
50. Kabsch, W. & Sander, C. (1983). Dictionary of protein secondary structure: pattern recognition of hydrogen-bonded and geometrical features. *Biopolymers*, **22**, 2577–2637.
51. Hun Lim, K., Nguyen, T. N., Damo, S. M., Mazur, T., Ball, H. L., Prusiner, S. B. *et al.* (2006). Solid-state NMR structural studies of the fibril form of a mutant mouse prion peptide PrP(89-143)(P101L). *Solid State Nucl. Magn. Reson.* **29**, 183–190.
52. Dominguez, C., Boelens, R. & Bonvin, A. M. (2003). HADDOCK: a protein-protein docking approach based on biochemical or biophysical information. *J. Am. Chem. Soc.* **125**, 1731–1737.
53. Zhang, C., Liu, S. & Zhou, Y. Q. (2004). Accurate and efficient loop selections by the DFIRE-based all-atom statistical potential. *Protein Sci.* **13**, 391–399.
54. Williamson, R. A., Peretz, D., Pinilla, C., Ball, H., Bastidas, R. B., Rozenshteyn, R. *et al.* (1998). Mapping the prion protein using recombinant antibodies. *J. Virol.* **72**, 9413–9418.
55. Prusiner, S. B., Scott, M., Foster, D., Pan, K. M., Groth, D., Mirenda, C. *et al.* (1990). Transgenetic studies implicate interactions between homologous PrP isoforms in scrapie prion replication. *Cell*, **63**, 673–686.
56. Cartoni, C., Schinina, M. E., Maras, B., Nonno, R., Vaccari, G., Di, M. *et al.* (2005). Identification of the pathological prion protein allotypes in scrapie-infected heterozygous bank voles (*Clethrionomys glareolus*) by high-performance liquid chromatography-mass spectrometry. *J. Chromatog. A*, **1081**, 122–126.
57. Supattapone, S., Muramoto, T., Legname, G., Mehlhorn, I., Cohen, F. E., De Armond, S. J. *et al.* (2001).

Identification of two prion protein regions that modify scrapie incubation time. *J. Virol.* **75**, 1408–1413.
58. Hill, A. F., Desbruslais, M., Joiner, S., Sidle, K. C., Gowland, I., Collinge, J. *et al.* (1997). The same prion strain causes vCJD and BSE. *Nature*, **389**, 448–450.
59. Telling, G. C., Scott, M., Hsiao, K. K., Foster, D., Yang, S. L., Torchia, M. *et al.* (1994). Transmission of Creutzfeldt-Jakob disease from humans to transgenic mice expressing chimeric human-mouse prion protein. *Proc. Natl Acad. Sci. USA*, **91**, 9936–9940.
60. Bossers, A., Belt, P., Raymond, G. J., Caughey, B., de Vries, R. & Smits, M. A. (1997). Scrapie susceptibility-linked polymorphisms modulate the in vitro conversion of sheep prion protein to protease-resistant forms. *Proc. Natl Acad. Sci. USA*, **94**, 4931–4936.
61. Goldmann, W., Hunter, N., Smith, G., Foster, J. & Hope, J. (1994). PrP genotype and agent effects in scrapie: change in allelic interaction with different isolates of agent in sheep, a natural host of scrapie. *J. Gen. Virol.* **75**, 989–995.
62. Kocisko, D. A., Priola, S. A., Raymond, G. J., Chesebro, B., Lansbury, P. T., Jr & Caughey, B. (1995). Species specificity in the cell-free conversion of prion protein to protease-resistant forms: a model for the scrapie species barrier. *Proc. Natl Acad. Sci. USA*, **92**, 3923–3927.
63. Thuring, C. M., Erkens, J. H., Jacobs, J. G., Bossers, A., Van Keulen, L. J., Garssen, G. J. *et al.* (2004). Discrimination between scrapie and bovine spongiform encephalopathy in sheep by molecular size, immunoreactivity, and glycoprofile of prion protein. *J. Clin. Microbiol.* **42**, 972–980.
64. Tremblay, P., Ball, H. L., Kaneko, K., Groth, D., Hegde, R. S., Cohen, F. E. *et al.* (2004). Mutant PrPSc conformers induced by a synthetic peptide and several prion strains. *J. Virol.* **78**, 2088–2099.
65. Manson, J. C., Jamieson, E., Baybutt, H., Tuzi, N. L., Barron, R., McConnell, I. *et al.* (1999). A single amino acid alteration (101L) introduced into murine PrP dramatically alters incubation time of transmissible spongiform encephalopathy. *EMBO J.* **18**, 6855–6864.
66. Chien, P., Weissman, J. S. & De Pace, A. H. (2004). Emerging principles of conformation-based prion inheritance. *Annu. Rev. Biochem.* **73**, 617–656.
67. Rost, B. (1995). TOPITS: threading one-dimensional predictions into three-dimensional structures. *Proc. Int. Conf. Intell. Syst. Mol. Biol.* **3**, 314–321.
68. Rost, B. (1996). PHD: predicting one-dimensional protein structure by profile-based neural networks. *Methods Enzymol.* **266**, 525–539.
69. Peitsch, M. C. (1996). ProMod and Swiss-Model: Internet-based tools for automated comparative protein modelling. *Biochem. Soc. Trans.* **24**, 274–279.
70. Hooft, R. W., Vriend, G., Sander, C. & Abola, E. E. (1996). Errors in protein structures. *Nature*, **381**, 272.
71. Lindahl, E., Hess, B. & van der Spoel, D. (2001). GROMACS 3.0: A package for molecular simulation and trajectory analisys. *J. Mol. Modeling*, **7**, 306–317.
72. Daura, X., Mark, A. E. & van Gunsteren, W. F. (1998). Parametrization of aliphatic CHn united atoms of GROMOS96 force field. *J. Comput. Chem.* **19**, 535–547.
73. Berendsen, H. J. C., Postma, J. P. M., van Gunsteren, W. F. & Hermans, J. (1981). Interaction models for water in relation to protein hydration. In *Intermolecular Forces* (Pullman, B., ed), pp. 331–342, Reidel Publishing Company, Dordrecht.
74. Berendsen, H. J. C., Postma, J. P. M., van Gunsteren, W. F., Di Nola, A. & Haak, J. R. (1984). Molecular dynamics with coupling to an external bath. *J. Chem. Phys.* **81**, 3684–3690.
75. Hess, B., Bekker, H., Berendsen, H. J. C. & Fraaije, J. G. E. M. (1997). LINCS: a linear constraint solver for molecular simulations. *J. Comput. Chem.* **18**, 1463–1472.
76. van Gunsteren, W. F. & Berendsen, H. J. C. (1990). Computer-simulation of molecular-dynamics-methodology, applications, and perspectives in chemistry. *Angew. Chem.-Int. Ed, English*, **29**, 992–1023.
77. Tironi, I. G., Sperb, R., Smith, P. E. & Vangunsteren, W. F. (1995). A generalized reaction field method for molecular-dynamics simulations. *J. Chem. Phys.* **102**, 5451–5459.
78. Hsu, S.-T. D. & Bonvin, A. M. J. J. (2004). Atomic insight into the CD4 binding-induced conformational changes in HIV-1 gp120. *Proteins: Struct. Funct. Genet.* **55**, 582–593.
79. Jorgensen, W. L. & Tirado-Rives, J. (1988). The OPLS potential functions for proteins. Energy minimizations for crystals of cyclin peptides and crambin. *J. Am. Chem. Soc.* **110**, 1657–1666.

Edited by M. Levitt

(Received 9 February 2006; received in revised form 12 May 2006; accepted 17 May 2006)
Available online 5 June 2006